inorganics

MDPI

Article

Fabrication and Characterization of 3D-Printed Porous Structures Based on Walstromite-Type Silicate Ceramics

Ștefania Caramarin [1,2], Lidia Licu [1], Florentina-Gabriela Ioniță [1], Andreea-Nicoleta Ghiță [1], Dumitru-Valentin Drăguț [1], Miruna-Adriana Ioța [1] and Laura-Mădălina Cursaru [1,*]

[1] National R&D Institute for Non-Ferrous and Rare Metals, 102 Biruintei Blvd, 077145 Pantelimon, Romania; schiriac@imnr.ro (Ş.C.); lidia.licu@imnr.ro (L.L.); gabriela.ionita@imnr.ro (F.-G.I.); andreea.ghita@imnr.ro (A.-N.G.); dragut@imnr.ro (D.-V.D.); iota.miruna@imnr.ro (M.-A.I.)
[2] Faculty of Chemical Engineering and Biotechnologies, National University of Science and Technology Politehnica Bucharest, 011061 Bucharest, Romania
* Correspondence: mpopescu@imnr.ro

Abstract: This study investigates the additive manufacturing of 3D porous scaffolds based on walstromite-type silicate ceramics for bone tissue engineering applications. Walstromite powders were synthesized using the sol-gel method and printed using extrusion-based 3D printing. Both sintered and unsintered scaffolds were characterized using scanning electron microscopy (SEM), Fourier transform infrared spectroscopy (FTIR), X-Ray diffraction (XRD) and energy dispersive X-ray spectroscopy (EDS) analyses to evaluate the effects of sintering on microstructure, porosity, and mechanical properties. Results indicate that the unsintered scaffolds exhibited significantly higher compressive strength due to the presence of organic binders, whereas the sintered scaffolds demonstrated enhanced porosity, facilitating cell infiltration and nutrient flow. Therefore, the sintering process reduced compressive strength, probably due to the loss of organic compounds and increased porosity. These findings underline the need for optimizing sintering parameters to balance mechanical integrity and porosity, ensuring that the scaffolds meet the mechanical and biological requirements for bone regeneration. Alternative sintering methods, such as microwave sintering, are also suggested for future research to minimize the mechanical degradation observed post-sintering.

Keywords: 3D printing; walstromite; sintering; ceramic scaffolds; porosity; mechanical properties

check for updates

Academic Editor: Kenneth J.D. MacKenzie

Received: 22 January 2025
Revised: 20 February 2025
Accepted: 22 February 2025
Published: 25 February 2025

Citation: Caramarin, Ș.; Licu, L.; Ioniță, F.-G.; Ghiță, A.-N.; Drăguț, D.-V.; Ioța, M.-A.; Cursaru, L.-M. Fabrication and Characterization of 3D-Printed Porous Structures Based on Walstromite-Type Silicate Ceramics. *Inorganics* **2025**, *13*, 68. https://doi.org/10.3390/inorganics13030068

Copyright: © 2025 by the authors. Licensee MDPI, Basel, Switzerland. This article is an open access article distributed under the terms and conditions of the Creative Commons Attribution (CC BY) license (https://creativecommons.org/licenses/by/4.0/).

1. Introduction

Additive manufacturing (AM), also known as 3D printing, has emerged as a transformative technology in materials science and biomedical engineering. Unlike traditional manufacturing methods, which often involve subtractive processes or molding techniques, AM builds structures layer by layer, allowing for unparalleled design flexibility and material efficiency [1]. This approach is particularly advantageous in applications requiring complex geometries and internal structures, such as the fabrication of scaffolds for bone tissue engineering. AM enables the precise control of porosity, pore size, and interconnectivity, which are crucial parameters for developing scaffolds that can support cell attachment, proliferation, and nutrient flow, ultimately promoting tissue regeneration [2].

One of the most significant advantages of additive manufacturing is its ability to create highly complex and customized designs that would be challenging or impossible to achieve through traditional methods [3]. For biomedical applications, particularly in bone tissue engineering, this capability is essential. The natural structure of bone is highly porous and

complex, with a specific architecture that provides mechanical support while allowing for vascularization and nutrient exchange [4]. AM techniques, such as robocasting or direct ink writing, can replicate these complex structures by creating scaffolds with controlled porosity and mechanical properties tailored to mimic the natural bone characteristics [5].

In addition to design flexibility, AM offers material efficiency and reduces waste, as it only uses the material necessary to build the structure. This is especially important when working with expensive or specialized materials, such as advanced ceramics, which are crucial in biomedical applications. Additive manufacturing also allows for the rapid prototyping and production of patient-specific implants, paving the way for personalized medicine. By utilizing 3D imaging data from a patient, it is possible to design and fabricate implants that match the patient's anatomy precisely, improving the fit, function, and integration of the implant with the surrounding tissue [6].

Ceramics, particularly those in the silicate family, have gained significant interest in bone tissue engineering due to their excellent biocompatibility, osteoconductivity, and mechanical properties [7]. Beyond their mechanical properties and biocompatibility, ceramics also exhibit excellent biotribological performance, making them suitable for applications in artificial organs. The sliding components of such medical devices, particularly in bone tissue engineering and joint replacements, benefit from the low friction and high wear resistance of ceramics. For instance, SiC ceramics have been studied for their tribological behaviour under lubrication, demonstrating superior wear resistance essential for long-term implant performance [8]. These properties further highlight the potential of ceramic materials in biomedical applications requiring both mechanical integrity and optimal tribological behaviour. Silicate ceramics, such as calcium silicates, can promote the formation of hydroxyapatite, a mineral that is the main component of natural bone, when in contact with body fluids. This characteristic makes them suitable candidates for bone regeneration applications [9]. Among these, walstromite, a barium-calcium silicate ($BaCa_2Si_3O_9$), stands out due to its unique combination of properties [10]. It offers a balance between mechanical strength and bioactivity, making it an ideal candidate for creating scaffolds that can support bone tissue growth.

Walstromite's ability to support the formation of new bone tissue while providing the necessary structural support is particularly valuable in load-bearing applications. The mineral composition of walstromite closely resembles the mineral phase of natural bone, enhancing its integration with the host tissue. Moreover, the degradation products of silicate ceramics like walstromite can release ions that stimulate cellular responses and promote bone formation, further enhancing their potential as scaffold materials [11].

In bone tissue engineering, the design of scaffolds with appropriate porosity is a critical factor. Porosity allows the ingrowth of cells and blood vessels, which is essential for the integration and maturation of the new tissue. The interconnected pore network in a scaffold provides pathways for the diffusion of nutrients and waste products, supporting cell viability and tissue formation [12]. Additionally, the mechanical properties of the scaffold, such as compressive strength and stiffness, can be adjusted by controlling the porosity, enabling the development of scaffolds that can withstand physiological loads [13].

Additive manufacturing techniques like robocasting enable the precise control of scaffold architecture, including the size, shape, and distribution of pores [14]. This level of control allows researchers to design scaffolds with optimized properties for specific applications. For example, a scaffold intended for load-bearing applications can be designed with a higher density and smaller pores to provide greater mechanical strength, while a scaffold intended for non-load-bearing applications can have a more open structure to enhance cell infiltration and tissue growth [15].

This research aims to explore the feasibility of using walstromite ceramics in additive manufacturing to create 3D porous scaffolds for bone tissue engineering. By capitalizing on the benefits of additive manufacturing, this study attempts to fabricate walstromite-based structures with controlled porosity and mechanical properties that can support bone regeneration. The sol-gel method has been employed to synthesize walstromite powders, which are further used in the robocasting process to create 3D structures. This approach offers the potential to develop scaffolds that not only provide the necessary mechanical support for bone tissue growth but also enhance the biological response, promoting faster and more effective healing.

2. Results and Discussion

2.1. Differential Scanning Calorimetry Analysis Results

To facilitate the debinding process (removal of the organic binders) aimed at increasing the porosity of the scaffolds and enhancing their mechanical strength [16], the green 3D-printed structures (shown in Figure 1) were first analysed by differential scanning calorimetry (DSC) in Ar atmosphere using a DSC 200 F3 Maia Netzsch equipment (Netzsch-Gerätebau GmbH, Selb, Germany). The thermal analysis was conducted up to a temperature of 600 °C, with a heating rate of 10 K/min and a cooling rate of 30 K/min.

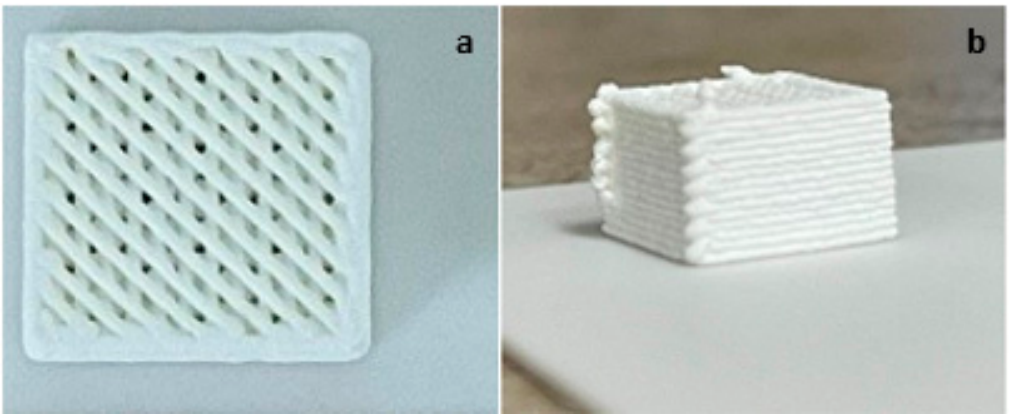


Figure 1. Examples of walstromite-based 3D-printed scaffolds: (**a**) 15 × 15 × 15 mm, (**b**) 10 × 10 × 10 mm.

The DSC analysis results presented in Figure 2 revealed three significant thermal events, as follows: (i) the first peak observed at 56.4 °C, with an enthalpy change (ΔH) of 7.662 J/g corresponds to an endothermic transition and could be assigned to the melting or softening of Pluronic F-127, a thermosensitive block copolymer used as binder in 3D printing process; (ii) a small endothermic peak occurred at 322.2 °C and could be related to the organic additives used in 3D printing process: either HPMC (Hydroxypropyl Methylcellulose) decomposition, as HPMC typically decomposes around this temperature, releasing volatile products, or thermal degradation of Baymedix FD103 (aqueous polyurethane dispersion); (iii) finally, the third peak at 397.8 °C, with an exothermic enthalpy (ΔH) of −40.46 J/g, suggests the oxidative degradation of residual organics, marking the final combustion of the polymeric matrix and effectively preparing the scaffold for sintering by removing any remaining organic binders.

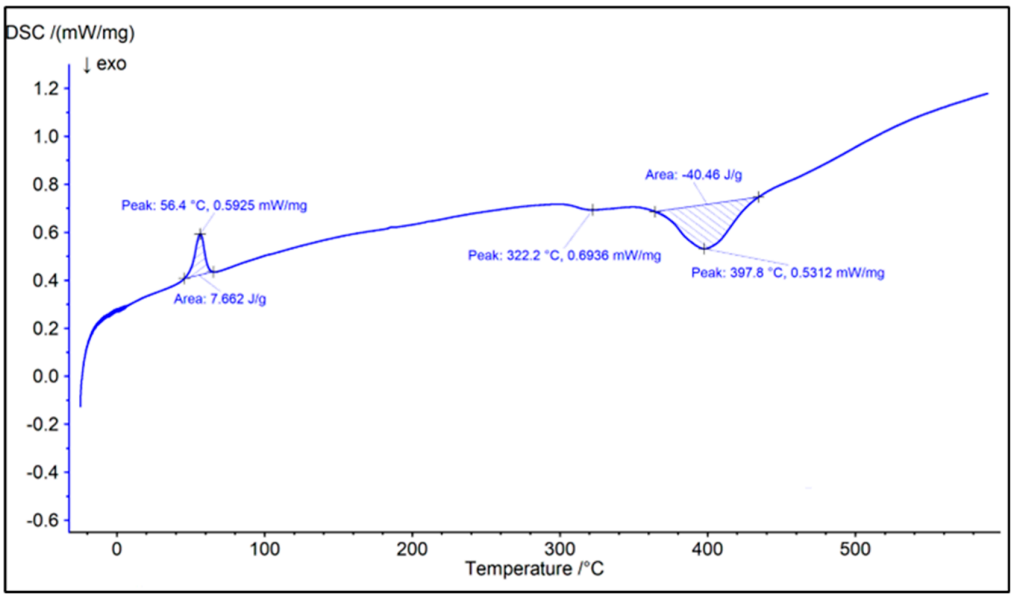


Figure 2. DSC curve of walstromite-based 3D green structures.

2.2. Amplitude Sweep Test Results

The shear-thinning behaviour of the walstromite ceramic paste, as observed in the amplitude sweep test results (Figure 3), is a fundamental characteristic for enabling smooth extrusion and deposition during the 3D printing process. Shear-thinning indicates that the paste becomes less viscous under shear stress, allowing it to flow easily through the nozzle and form fine, controlled layers. However, while shear-thinning is an essential characteristic for printability, it is not sufficient on its own to guarantee the success of the printing process.

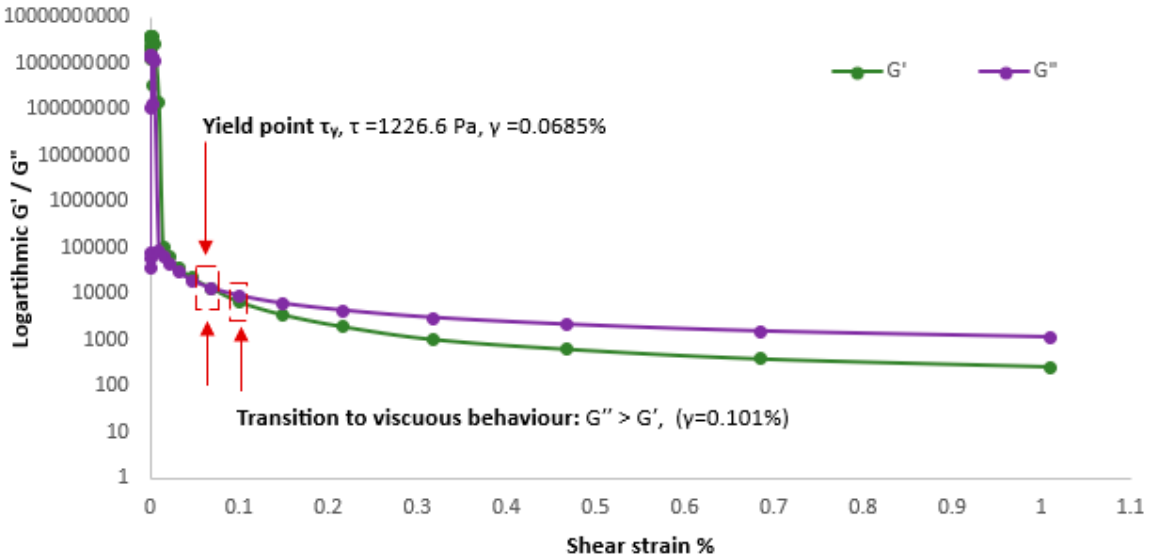


Figure 3. Graphic representation of G′, G″ as a function of shear strain for walstromite-based ceramic paste.

The yield point of a material, which is defined as the stress at which the material transitions from a solid-like behaviour (viscoelastic solid) to a more fluid-like behaviour (viscoelastic liquid), is also crucial for 3D printing. The yield point is directly linked to the formation of stable, well-defined layers in 3D printing. A yield point greater than 1×10^3 Pa ensures that the paste can withstand the forces applied during deposition without collapsing or losing its structure [17]. This is particularly important in processes like robocasting, where

the material is extruded layer by layer to form complex 3D shapes. When the yield point is too low, the material may flow excessively, leading to poor shape fidelity, distortion, or slumping. Conversely, a higher yield point helps maintain the integrity of the printed structures, ensuring the deposited material retains its shape immediately after extrusion. In this context, the walstromite paste demonstrated a yield point of 1226.6 Pa, well above the threshold of 1×10^3 Pa. This confirms that the paste has sufficient strength to maintain shape retention and self-supporting capabilities during the printing process.

The data in Figure 3 also indicate that the storage modulus G′ increases significantly with shear strain, reflecting the material's ability to store elastic energy and resist deformation under stress. The oscillatory rheology of the paste shows a gradual transition from a solid-like to a more fluid-like behaviour as the shear stress increases. This gradual shift is advantageous for the printing process, as it provides a balance between extrudability and structural integrity. A more gradual transition ensures that the paste can be easily extruded at lower shear stresses but will retain its shape when printed at higher strain levels, where the material must be stable enough to build up layers without deforming. The paste's yield point, combined with the shear-thinning behaviour, guarantees that the printed scaffold will possess the necessary mechanical strength for load-bearing applications in bone tissue engineering. The ability to maintain shape retention and self-supporting capabilities during printing directly impacts the mechanical properties of the final product, which are critical in ensuring that the scaffold can endure the physiological loads in vivo.

2.3. BET Specific Surface Results

The sintered 3D-printed scaffold analysed through nitrogen adsorption-desorption isotherms (Figure 4) exhibited a low surface area of 1.18 m^2/g, indicating the macroporosity of the sample. According to the IUPAC classification, the sintered 3D-printed structure has a Type III isotherm, suggesting a typical macroporous structure. The BJH (Barrett-Joyner-Halenda) analysis showed a broad pore size distribution, with pores ranging from 1.7 nm (micropores) to 250 nm (macropores) and a cumulative pore volume of 0.0025 cm^3/g (Figure 5). These features reflect the scaffold's macroporosity, which is critical for cell attachment, nutrient transport, and vascularization in tissue engineering applications. The scaffold's pore architecture, while not predominantly mesoporous, provides sufficient porosity to facilitate moderate adsorption properties, which can be advantageous in tissue engineering and drug delivery applications.

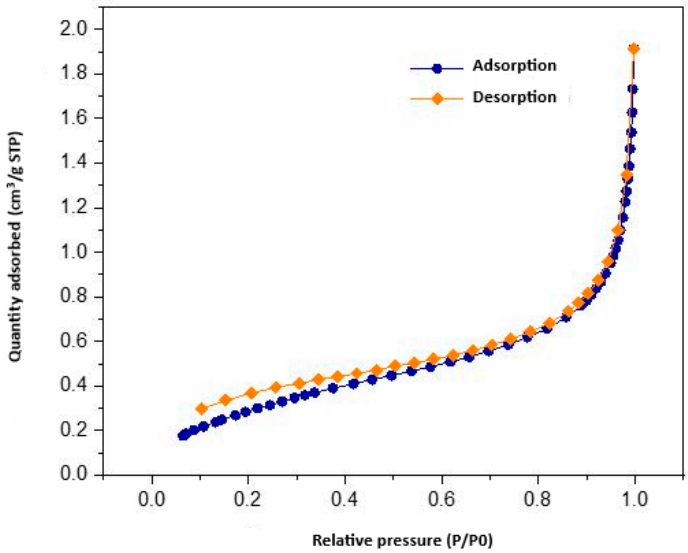


Figure 4. Adsorption-desorption isotherm for sintered 3D-printed structures based on walstromite.

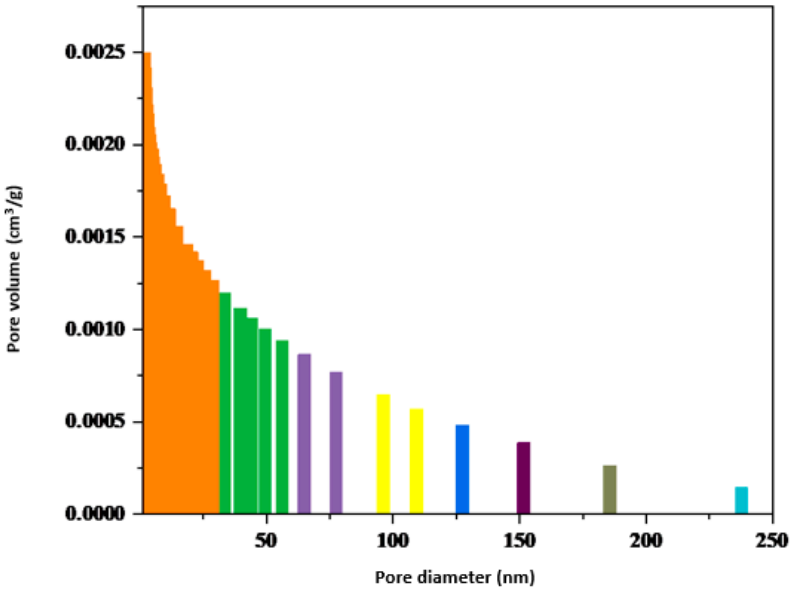


Figure 5. BJH pore distribution for sintered 3D-printed structures based on walstromite.

2.4. Fourier Transformed Infrared Spectroscopy (FTIR) Results

The FTIR spectra of both sintered (3D 1.7-6) and unsintered (3D 1.7-12) walstromite-based scaffolds, as depicted in Figure 6, reveal key insights into the material composition and structural changes during processing.

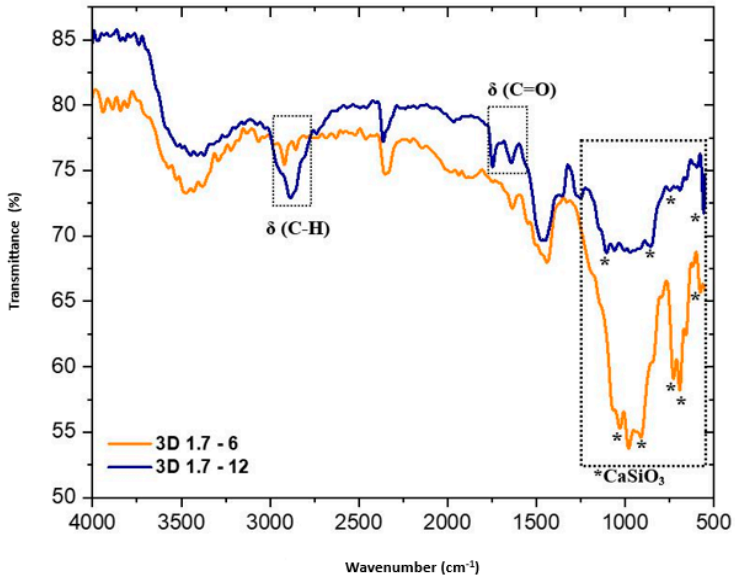


Figure 6. The FTIR spectra for sintered (3D 1.7-6) and unsintered (3D 1.7-12) walstromite-based 3D-printed scaffolds.

The unsintered sample (3D 1.7-12) exhibits several peaks associated with organic additives. The characteristic peaks in the region of 2900–2950 cm^{-1} correspond to C-H stretching vibrations from aliphatic hydrocarbon chains, which are often associated with polymeric binders or plasticizers used during the 3D printing process. The sharp peak around 1700–1750 cm^{-1} is indicative of C=O stretching vibrations, typically attributed to carbonyl groups. These signals point out the presence of organic compounds, likely remnants of binders, which are essential for maintaining the structural integrity of the green body before sintering.

In the sintered sample (3D 1.7-6), the disappearance of the C-H and C=O peaks confirms the successful removal of organic additives through the debinding process, which typically involves the decomposition and evaporation of these components during the early stages of sintering. This indicates that the sintering process was effective in eliminating the organic content, ensuring the purity of the ceramic scaffold. The absence of these peaks also suggests that no significant residue from the organic phase remains, which is critical for producing a mechanically strong and biocompatible ceramic structure.

Both the sintered and unsintered samples exhibit strong peaks in the 500–1200 cm^{-1} region, which are characteristic of the walstromite ceramic phase. Specifically, these peaks correspond to the Si-O stretching and bending vibrations, as well as the metal-oxygen bond vibrations (such as Ca-O or Ba-O) [18–20] that are integral to the walstromite structure. The walstromite phase, being a barium-calcium silicate, typically shows these spectral features due to its silicate framework. Notably, the intensity and position of these peaks are slightly different in the sintered sample, suggesting that the sintering process has induced some structural reorganization. This could be due to the densification and phase transformations commonly observed during sintering, where the crystal structure becomes more ordered with minimized defects. Such changes are typical in ceramic materials during sintering, as higher temperatures drive diffusion processes that can result in grain growth and the elimination of porosity, leading to an overall alteration in the vibrational characteristics of the material.

2.5. X-Ray Diffraction Results

The sintered 3D structures were characterized using X-ray diffraction analysis to identify the crystalline phases present in the investigated sample. The obtained results are depicted in Table 1 and Figure 7.

Table 1. Crystalline compounds identified by XRD analysis.

Compound Name	PDF Reference	Chemical Formula	Crystallization System	Semi-Quantitative Analysis
Barium-Calcium Silicate	040-149-1111	$Ba_{1-x}Ca_xSiO_4$	Hexagonal	≈14.7%
Walstromite	04-025-3409	$BaCa_2Si_3O_9$	Triclinic	≈52.4%
Cristobalite	00-071-0087	SiO_2	Tetragonal	≈3.8%
Barium-Silicon Oxide	04-009-1825	$BaSi_2O_5$	Monoclinic	≈8.8%
Ca_2SiO_4	04-012-6734	Ca_2SiO_4	Orthorhombic	≈20.4%

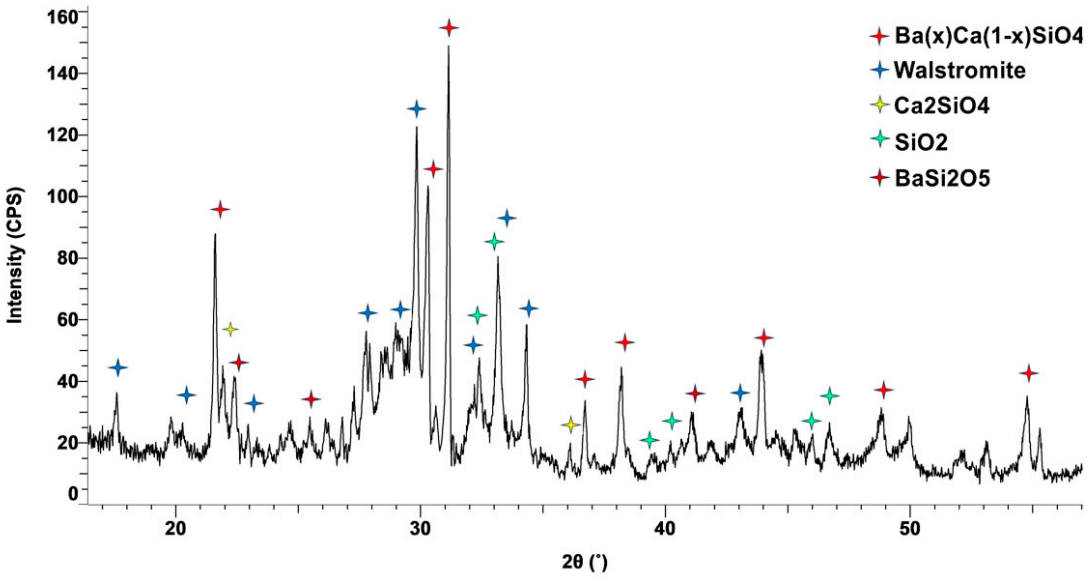


Figure 7. Diffractogram of a walstromite-based sintered 3D structure.

The semi-quantitative phase analysis was performed, considering the fact that all the phases are crystalline and are detected. The analysis refers only to the presence of the crystalline phase, neglecting the amorphous content. The analysis was performed using the Relative Intensity Ratio (RIR) [21]. As shown in Table 1, the compound of interest, walstromite, represents the predominant phase, accounting for over 52% of the total crystalline phases.

2.6. SEM Microscopy Results

3D-printed scaffolds based on walstromite before and after sintering were studied by scanning electron microscopy. The obtained images are presented in Figure 8 at two magnifications: 70× (Figure 8a,c) and 5000× (Figure 8b,d). Both samples are formed by several layers of successively deposited strands, visible in Figure 8a,c, at lower magnification (70×). The strands are made up of porous granular aggregates of irregular shape, with tens of micrometres in size, visible in Figure 8b,d, at higher magnification (5000×). In the case of the sintered sample (Figure 8c), the strands have a rough appearance and show transversely oriented cracks.

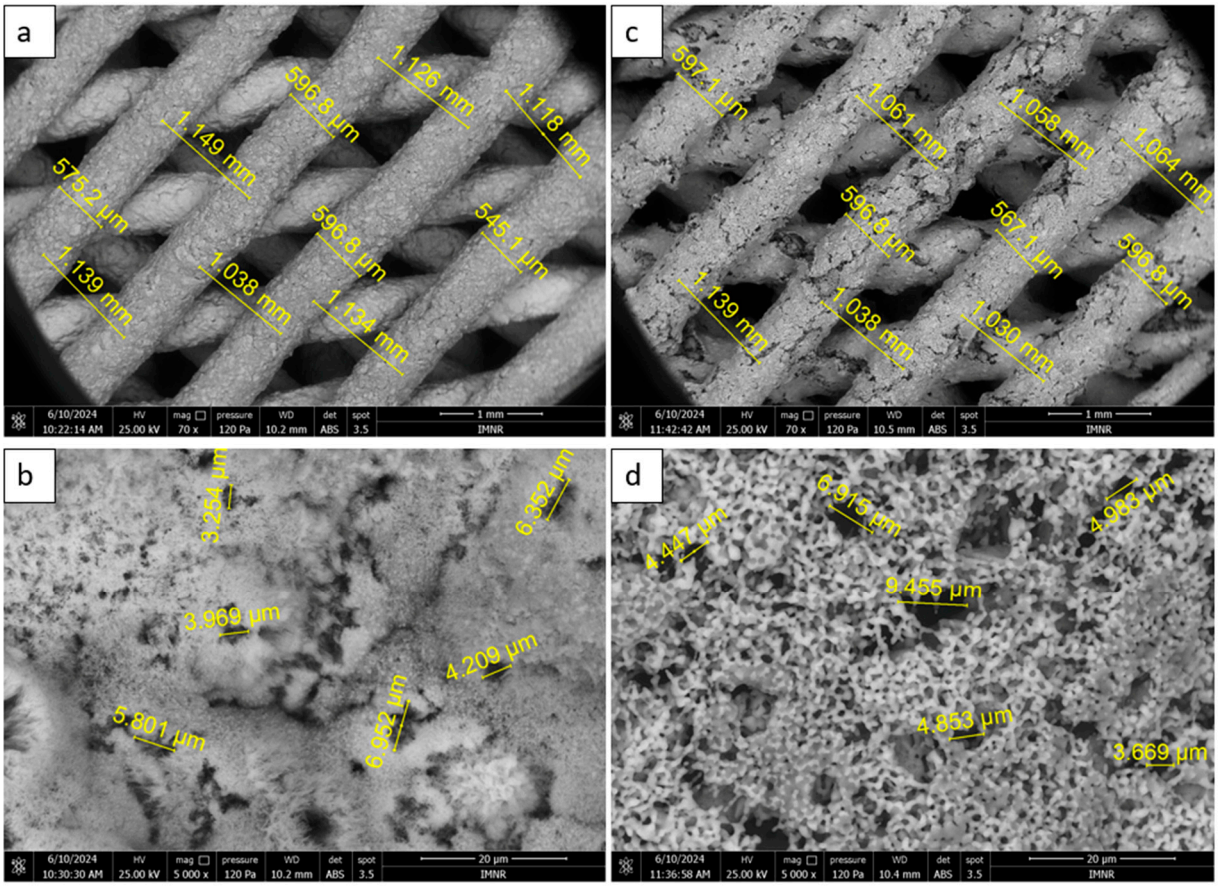


Figure 8. SEM images for the 3D structures based on walstromite: (**a**,**b**) before sintering; (**c**,**d**) after sintering.

In Figure 8a,c, both the spacing (denoted as d) between the deposited strands and their thickness (denoted as g) can be observed. The spacing (d) ranges from 1.03 to 1.15 mm, which is consistent with the 1.2 mm spacing set in the printer Visual Machines software (Version 2.10.130r5). It is also notable that the strand thickness varies between 550 and 597 µm, in line with the 600 µm inner diameter of the nozzle used to extrude the walstromite-based paste. The small differences observed for both d and g compared to the Visual Machines

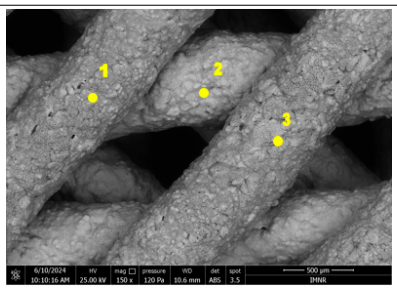
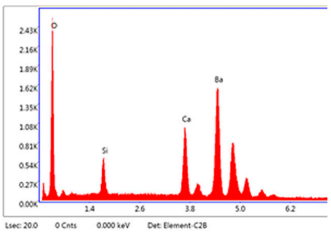
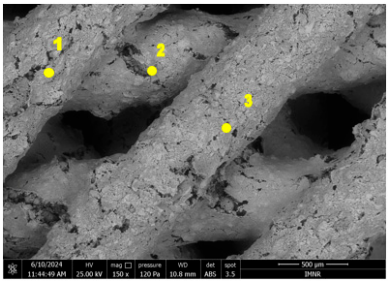
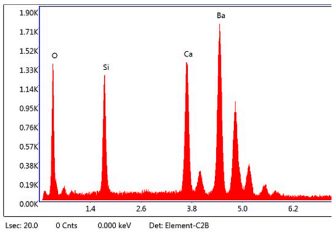
software (Version 2.10.130r5) settings are due to shrinkage that occurs during the drying of the samples.

Additionally, comparing Figure 8b,d, we observe that before sintering (Figure 8b), the structure exhibits a predominantly amorphous appearance due to the polymers used in the paste composition. In contrast, after sintering (Figure 8d), the debinding process becomes evident (the amorphous appearance from the polymers is no longer present), and the walstromite crystalline grains are more clearly defined. Also, regarding the porosity, in Figure 8b (before sintering), the pores are relatively larger and display less uniformity and connectivity, resulting in a structure with varied pore sizes (4–7 µm). After debinding, as shown in Figure 8d, the pores become more uniform in size (around 4 µm) and exhibit enhanced connectivity. This refinement in pore structure is crucial for tissue engineering applications, as a more consistent and interconnected porosity can facilitate better cell infiltration, nutrient transport, and overall scaffold integration, thereby improving the material's suitability for bone tissue engineering.

Thus, the SEM images effectively demonstrate the changes in the microstructure of the 3D-printed walstromite-based scaffolds before and after sintering. The sintering process appears to maintain the overall strand dimensions but introduces additional cracks and alters the pore structure. The strand roughness remains consistent, suggesting it is a feature inherent to the material or the manufacturing process.

The 3D structures were also characterized by energy-dispersive X-ray spectroscopy, an analytical technique used for sample elemental analysis or chemical characterization based on SEM images. EDS results highlighted the presence of specific elements for walstromite—O, Si, Ba, and Ca —in both types of structures (sintered or non-sintered). The mass percentages related to each point analysed are presented in Table 2.

Table 2. EDS analysis results for walstromite-based 3D structures.

Unsintered 3D Scaffold		**SPOT**	**Ba**	**Ca**	**Si**	**O**
			Atomic %			
		1	12.20	7.70	5.78	74.32
		2	16.04	7.13	6.09	70.74
		3	17.51	10.34	7.00	65.15
Sintered 3D Scaffold		**SPOT**	**Ba**	**Ca**	**Si**	**O**
			Atomic %			
		1	19.25	15.96	18.50	46.29
		2	19.52	13.11	17.55	49.82
		3	23.50	16.95	19.99	39.56

2.7. Mechanical Resistance Test Results

To evaluate the mechanical behaviour of the walstromite-based 3D-printed structures, both sintered (3D 1.7-8) and unsintered (3D 1.7-7) structures were subjected to a mechanical

compressive strength test. The obtained results are presented in Figure 9. As observed, the unsintered 3D structure exhibits significantly higher compressive strength compared to the sintered structure. This suggests that the presence of organic binders/additives contributes to the initial mechanical strength. Furthermore, the sintering process appears to significantly reduce the compressive strength of the 3D structure. This reduction in strength can be attributed to the loss of organic compounds and potential microstructural changes, such as increased porosity or grain growth, which is also confirmed by the SEM images in Figure 8.

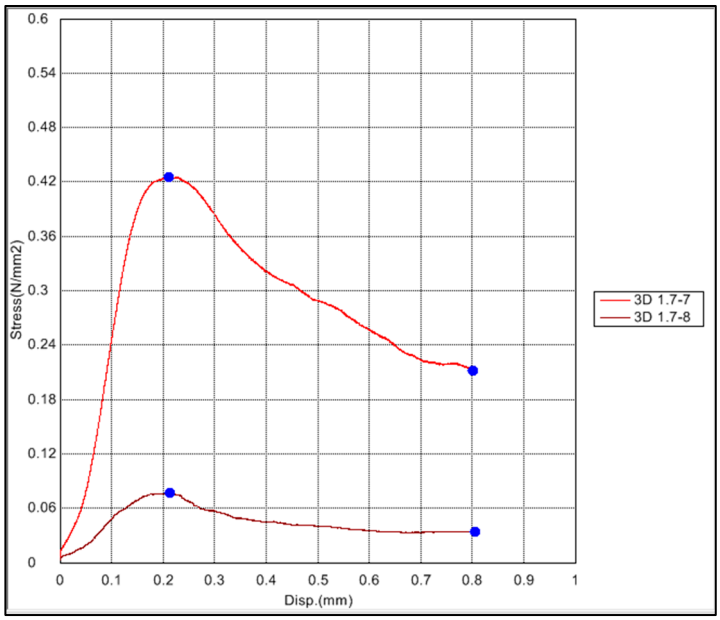


Figure 9. Compressive strength test results for walstromite-based 3D structures: unsintered (3D 1.7-7) and sintered (3D 1.7-8).

From the perspective of final applications, scaffolds for bone tissue engineering must possess adequate compressive strength to support load-bearing applications. Therefore, the unsintered structure demonstrates higher initial strength due to the presence of organic additives, though the biocompatibility of these components must be carefully evaluated. While sintering may improve biocompatibility by removing these organic compounds, it comes at the cost of reduced mechanical strength.

Additionally, porosity is a crucial factor for cell infiltration and nutrient flow. The sintered structure may offer better porosity, albeit at the expense of mechanical integrity. Thus, balancing porosity with mechanical strength is essential, which makes optimizing sintering parameters (temperature, time, atmosphere) necessary to minimize strength loss while achieving the desired microstructure and porosity. Alternative sintering techniques, such as microwave sintering or spark plasma sintering, could be considered to address these challenges.

3. Materials and Methods

3.1. Walstromite Sol-Gel Synthesis

To obtain walstromite powder ($BaCa_2Si_3O_9$), Ca $(NO_3)_2$*$4H_2O$ and Ba (NO_3) precursors are dissolved in ethanol solution. Simultaneously, TEOS (tetraethyl-orthosilicate) is hydrolysed in distilled water, and 65% HNO_3 is added until a pH of 2–2.5 is reached. The hydrolysed TEOS solution is then slowly dripped into the salt solution and homogenized gently on a hot plate (80 °C). After the gel is formed, it is left to mature at room temperature for 24 h and then dried in an oven at 100 °C for 12 h. Finally, the powder is calcined at 750

°C for 4 h, with a heating/cooling rate of 10 °C/min in an electric furnace. The obtained powder has a particle size of 1.02–1.04 μm (according to the results obtained with a fully automated Micromeritics® TriStar II Plus system, Norcross-Atlanta, GA, USA).

3.2. Preparation of Walstromite-Based Pastes for 3D Printing

The preparation of the paste required for 3D printing walstromite-based scaffolds involves mixing 60% walstromite powder with 40% binder solution made by combining three commercial organic additives: Baymedix FD103 (aqueous polyurethane dispersion), a 15% HPMC (hydroxypropyl methylcellulose) solution and a 30% Pluronic F-127 solution. The mixture is homogenized using a Thinky-ARE 250 planetary centrifugal mixer (Thinky Corporation, Tokyo, Japan) for 6 min at 2000 rpm. Following this, the same mixer is used for a defoaming step to remove any air bubbles, which could otherwise compromise the quality of the 3D printing process. The resulting homogeneous pastes were then used for the additive manufacturing of 3D structures with the 3D-Bioplotter EnvisionTEC Starter System (EnvisionTEC GmbH, Gladbeck, Germany).

3.3. Additive Manufacturing of 3D Structures Based on Walstromite Pastes

Walstromite-based scaffolds were produced by the extrusion-based 3D printing technique using the 3D-BioPlotter Starter Series system (EnvisionTEC GmbH, Germany), connected to a computer equipped with the necessary software (Visual Machines software (Version 2.10.130r5)) for importing STL data and controlling the printer. After importing the STL files (which were obtained using a CAD design software—SolidWorks 19, Version 2019 SP0.0), the following working parameters were set: cubic structures with dimensions of 15 × 15 × 15 mm and 10 × 10 × 10 mm, strand distance of 1.2 mm, nozzle diameter of 600 μm, angle between layers of 45°, working temperature of 26 °C, applied pressure of 2–3 bar and an extrusion speed ranging from 16 to 20 mm/s.

3.4. Post-Printing Treatment of Walstromite 3D Scaffolds

Based on the DSC analysis results (Figure 2), a thermal treatment protocol was established, involving heating the 3D structures from room temperature to 1100 °C (Figure 10). This was carried out using a Carbolite Gero furnace (30–3000 °C) from Verder Scientific, equipped with a digital programmer.

The thermal treatment protocol for the 3D-printed scaffolds based on walstromite with organic additives (Pluronic, HPMC, and Baymedix) follows a well-structured multi-step heating process designed to ensure efficient debinding and proper sintering. This protocol takes into account the various thermal transitions of the additives observed from the DSC analysis, specifically targeting the key decomposition and combustion points of the organic components while maintaining the integrity of the walstromite scaffold.

In the initial stage, the scaffold is heated to 60 °C and held for 30 min. This step is crucial for removing any residual moisture within the scaffold, ensuring that water evaporation does not disrupt the subsequent heating stages. Moisture can often lead to micro-cracks or structural defects if removed too quickly. Hence, this low-temperature hold allows for a controlled, gradual release of water vapor.

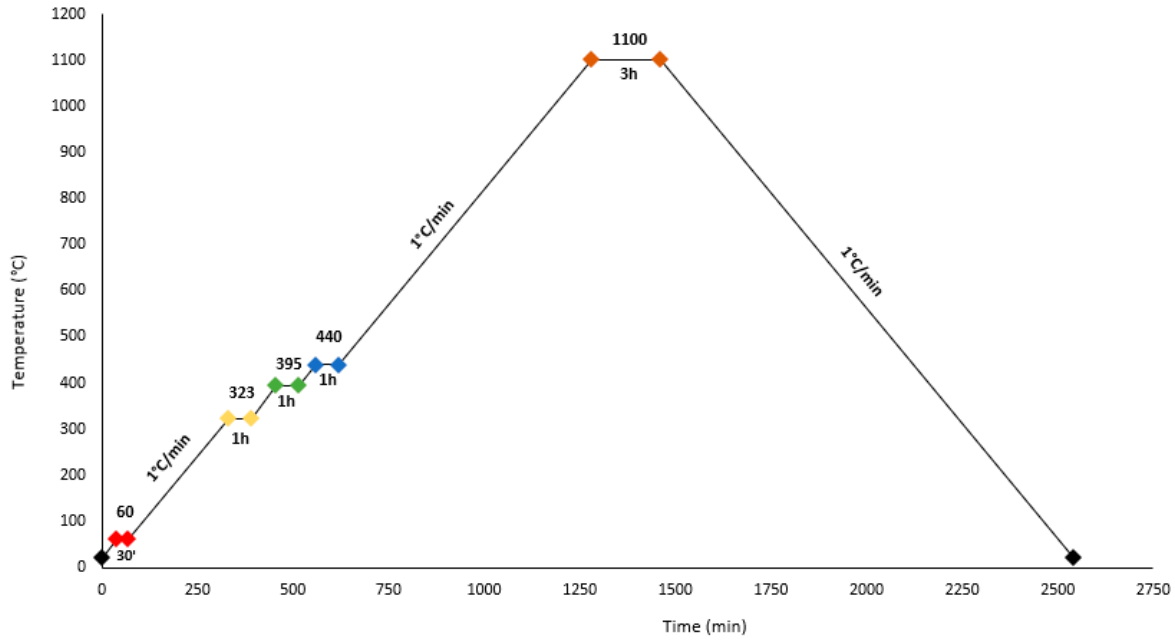


Figure 10. The five-step sintering program for walstromite-based 3D structures.

Following the moisture removal, the scaffold is heated to 323 °C for 1 h. This temperature correlates with the second peak seen in the DSC analysis (322.2 °C), where a significant endothermic transition occurs due to the thermal degradation of the organic additives, such as HPMC and Baymedix. Holding at this temperature ensures that most of these polymeric binders are fully degraded and volatilized, preventing incomplete decomposition that could interfere with later stages of sintering.

The next stage increases the temperature to 395 °C for 1 h, which corresponds closely with the third peak observed in the DSC data (397.8 °C). This step plays a vital role in eliminating any remaining organic residues. The exothermic nature of this peak suggests that oxidative degradation is occurring, ensuring complete combustion of any remaining carbonaceous material. This phase is essential for ensuring that the scaffold is clean and free of organic contaminants before the sintering process begins.

The protocol then transitions to 440 °C for 1 h, providing a final heating stage to ensure that any minor residues from the organic additives are fully removed. While this temperature is slightly beyond the range identified in the DSC analysis, it acts as a safety margin to ensure thorough debinding. This helps avoid any residual organics that might otherwise disrupt the structural integrity of the scaffold during high-temperature sintering.

Finally, the scaffold is heated to the sintering temperature of 1100 °C and held for 3 h. This extended high-temperature hold allows the walstromite to undergo proper densification and crystallization, achieving the necessary mechanical strength and microstructural properties. The slow ramping and long holding times at this stage prevent thermal shocks and potential cracking, allowing for uniform sintering across the scaffold structure.

3.5. Characterization Methods

3.5.1. Printability Evaluation of the Walstromite Ceramic Paste by Amplitude Sweep Test

An amplitude sweep test is crucial for understanding the viscoelastic properties of the ceramic paste before printing. This test not only measures the elastic (G′) and viscous (G″) moduli but also reveals how the material behaves under varying shear conditions. By determining the yield point and the behaviour of the paste within different amplitude ranges, we can assess its stability and ability to maintain structure during the printing process. If the paste does not demonstrate the required mechanical properties, it may

result in poor layer adhesion or deformation during printing, ultimately affecting the final product quality [22].

For the ceramic paste based on walstromite, an amplitude sweep test was conducted using the Anton Paar MCR 302e rheometer (Anton Paar, Graz, Austria) equipped with a PP25 plate-plate measurement system (SN100321). The test was performed at a constant angular frequency of $\omega = 1$ rad/s and maintained at a constant temperature of T = 26 °C.

3.5.2. BET Specific Surface Measurement

The sintered 3D structures based on walstromite were analysed using BET (Brunauer-Emmett-Teller) methodology to determine their specific surface area and porosity. This analysis was conducted with a high-precision, fully automated Micromeritics® TriStar II Plus system (Norcross, GA, USA). Prior to analysis, the samples were degassed at 300 °C for 3 h. The analysis was conducted in a nitrogen atmosphere, utilizing adsorption-desorption isotherms at 77 K.

3.5.3. Structural Characterization by Fourier Transformed Infrared Spectroscopy (FTIR)

The presence of characteristic chemical bonds was assessed by Fourier transform infrared spectroscopy (FT-IR) with an ABB MB 3000 spectrometer (ABB Inc., Québec, QC, Canada). The spectra were acquired at room temperature between 4000 and 550 cm^{-1} for both green and sintered 3D structures.

3.5.4. Characterization by X-Ray Diffraction

The sintered 3D structures were also characterized using X-ray diffraction analysis to identify the existing phases. Data acquisition was performed on a BRUKER D8 ADVANCE diffractometer utilizing DIFFRACplus XRD Commander software (DIFFRAC.EVA VER.5 2019) (Bruker AXS, Karlsruhe, Germany). The measurements were conducted using the Bragg-Brentano diffraction method in a vertical θ-θ configuration.

3.5.5. Morpho-Structural Characterization by Scanning Electron Microscopy (SEM)

The morphology of both the green and sintered 3D-printed scaffolds was examined using scanning electron microscopy (SEM) with a Quanta 250 high-resolution microscope (FEI Company, Eindhoven, The Netherlands). This setup was equipped with an energy-dispersive X-ray spectrometer (EDS) from EDAX (Mahwah, NJ, USA), featuring a fixed ELEMENT Silicon Drift Detector and the APEX™ 1.0 EDS Analysis Software Suite. Both samples were analysed in Low Vacuum (LV) mode utilizing the Backscattered Secondary Electron (ABS) detector.

3.5.6. Mechanical Resistance Measurement

To assess the mechanical behaviour of the 3D-printed structures based on walstromite, both the green and sintered samples were subjected to a compressive strength test using a Shimadzu Autograph AGS-X 20 kN testing machine (Shimadzu, Tokyo, Japan).

4. Conclusions

In this study, the potential of walstromite-based 3D-printed scaffolds for bone tissue engineering was explored, with a focus on the effects of sintering on mechanical properties and microstructural changes. The unsintered structures demonstrated higher compressive strength, likely due to the presence of organic binders that contribute to initial mechanical stability. However, the sintering process, while improving biocompatibility by removing these organic components, significantly reduced compressive strength. This reduction can be attributed to microstructural changes, such as increased porosity and grain growth, as confirmed by SEM analysis.

The sintered scaffolds, while mechanically weaker, exhibited improved porosity, which is crucial for cellular infiltration and nutrient flow—key factors for successful bone regeneration. Therefore, optimizing the balance between mechanical integrity and porosity is essential for tailoring these scaffolds for specific biomedical applications.

Further work will focus on refining sintering parameters or exploring alternative techniques, such as microwave or spark plasma sintering, to minimize the loss in mechanical properties while achieving the desired scaffold architecture.

Biocompatible properties of the 3D-printed scaffolds will also be tested to find the most appropriate application of this material in bone tissue engineering.

Overall, these findings highlight the potential of additive manufacturing for creating customizable, walstromite-based scaffolds that combine adequate mechanical support with the required biological functionality, paving the way for their application in bone tissue engineering.

Author Contributions: Conceptualization, Ş.C. and L.-M.C.; methodology, Ş.C. and L.-M.C.; software, L.L.; investigation, L.L., F.-G.I., A.-N.G., D.-V.D. and M.-A.I.; data curation, Ş.C.; writing—original draft preparation, Ş.C.; writing—review and editing, L.-M.C.; project administration, L.-M.C. All authors have read and agreed to the published version of the manuscript.

Funding: This research was funded by Ministry of Research, Innovation and Digitization (MCID), Core Program 5N/01.01.02023-ENERCLEAN, grant number PN 23250201/2023.

Data Availability Statement: The original contributions presented in the study are included in the article. Further inquiries can be directed to the corresponding author.

Conflicts of Interest: The authors declare no conflicts of interest.

References

1. Bera, T. A Review on Significant Role of Additive Manufacturing in Biomedical Applications. *Adv. Mater. Sustain. Manuf.* **2024**, *1*, 10002. [CrossRef]
2. Selim, M.; Mousa, H.M.; Abdel-Jaber, G.T.; Barhoum, A.; Abdal-hay, A. Innovative Designs of 3D Scaffolds for Bone Tissue Regeneration: Understanding Principles and Addressing Challenges. *Eur. Polym. J.* **2024**, *215*, 113251. [CrossRef]
3. Attaran, M. The Rise of 3-D Printing: The Advantages of Additive Manufacturing over Traditional Manufacturing. *Bus. Horiz.* **2017**, *60*, 677–688. [CrossRef]
4. Zhou, J.; Xiong, S.; Liu, M.; Yang, H.; Wei, P.; Yi, F.; Ouyang, M.; Xi, H.; Long, Z.; Liu, Y.; et al. Study on the Influence of Scaffold Morphology and Structure on Osteogenic Performance. *Front. Bioeng. Biotechnol.* **2023**, *11*, 1127162. [CrossRef] [PubMed]
5. Palivela, B.C.; Bandari, S.D.; Mamilla, R.S. Extrusion-Based 3D Printing of Bioactive Glass Scaffolds-Process Parameters and Mechanical Properties: A Review. *Bioprinting* **2022**, *27*, e00219. [CrossRef]
6. Oladapo, B.I.; Olawumi, M.A.; Omigbodun, F.T. Advancements and Future Prospects of Additive Manufacturing in Orthopedics. In *Medical Additive Manufacturing: Concepts and Fundamentals*; Elsevier: Amsterdam, The Netherlands, 2024; pp. 443–473. ISBN 9780323953832.
7. Youness, R.A.; Tag El-deen, D.M.; Taha, M.A. A Review on Calcium Silicate Ceramics: Properties, Limitations, and Solutions for Their Use in Biomedical Applications. *Silicon* **2023**, *15*, 2493–2505. [CrossRef]
8. Zhang, W. Tribology of SiC Ceramics under Lubrication: Features, Developments, and Perspectives. *Curr. Opin. Solid State Mater. Sci.* **2022**, *26*, 101000. [CrossRef]
9. Liu, Z.; He, X.; Chen, S.; Yu, H. Advances in the Use of Calcium Silicate-Based Materials in Bone Tissue Engineering. *Ceram. Int.* **2023**, *49*, 19355–19363. [CrossRef]
10. Raut, S.K.; Dhoble, N.S.; Park, K.; Dhoble, S.J. Precipitation Based Synthesis and Luminescence of Ln^{3+} (Eu, Ce, Dy, Sm, Tb) Activated $BaCa_2Si_3O_9$-Walstromite Cyclosilicate Phosphors. *Mater. Chem. Phys.* **2014**, *147*, 594–603. [CrossRef]
11. Chiriac, Ş.; Popescu, R.C.; Pele, M.M.; Ghiţulică, C.D.; Cucuruz, A.; Geanaliu-Nicolae, R.E.; Stancu, I.C.; Voicu, G.; Ciocan, L.T. New 3D Printed Scaffolds Based on Walstromite Synthesized by Sol–Gel Method. *J. Funct. Biomater.* **2024**, *15*, 19. [CrossRef]
12. Mohammadi, H.; Sepantafar, M.; Muhamad, N.; Bakar Sulong, A. How Does Scaffold Porosity Conduct Bone Tissue Regeneration? *Adv. Eng. Mater.* **2021**, *23*, 2100463. [CrossRef]
13. Miri, Z.; Haugen, H.J.; Loca, D.; Rossi, F.; Perale, G.; Moghanian, A.; Ma, Q. Review on the Strategies to Improve the Mechanical Strength of Highly Porous Bone Bioceramic Scaffolds. *J. Eur. Ceram. Soc.* **2024**, *44*, 23–42. [CrossRef]

14. Lewis, J.A. Direct Ink Writing of 3D Functional Materials. *Adv. Funct. Mater.* **2006**, *16*, 2193–2204. [CrossRef]
15. Cheng, A.; Schwartz, Z.; Kahn, A.; Li, X.; Shao, Z.; Sun, M.; Ao, Y.; Boyan, B.D.; Chen, H. Advances in Porous Scaffold Design for Bone and Cartilage Tissue Engineering and Regeneration. *Tissue Eng. Part. B Rev.* **2019**, *25*, 14–29. [CrossRef]
16. Shahzad, A.; Lazoglu, I. Direct Ink Writing (DIW) of Structural and Functional Ceramics: Recent Achievements and Future Challenges. *Compos. B Eng.* **2021**, *225*, 109249. [CrossRef]
17. Bonilla-Cruz, J.; Ávila-López, M.A.; Rodríguez, F.E.L.; Aguilar-Elguezabal, A.; Lara-Ceniceros, T.E. 3D Printable Ceramic Pastes Design: Correlating Rheology & Printability. *J. Eur. Ceram. Soc.* **2022**, *42*, 6033–6039. [CrossRef]
18. Zhu, Z.; Wang, Z.; Zhou, Y.; Chen, Y.; Zhou, L.; She, A. Evaluation of the Nanostructure of Calcium Silicate Hydrate Based on Atomic Force Microscopy-Infrared Spectroscopy Experiments. *Nanotechnol. Rev.* **2021**, *10*, 807–818. [CrossRef]
19. Eniu, D.; Gruian, C.; Vanea, E.; Patcas, L.; Simon, V. FTIR and EPR Spectroscopic Investigation of Calcium-Silicate Glasses with Iron and Dysprosium. *J. Mol. Struct.* **2015**, *1084*, 23–27. [CrossRef]
20. John, E.; Stephan, D. Calcium Silicate Hydrate—In-Situ Development of the Silicate Structure Followed by Infrared Spectroscopy. *J. Am. Ceram. Soc.* **2021**, *104*, 6611–6624. [CrossRef]
21. DIFFRAC. *EVALUATION PACKAGE. DIFFRAC.EVA User's Manual*; Bruker AXS GmbH: Karlsruhe, Germany, 2021.
22. del-Mazo-Barbara, L.; Ginebra, M.P. Rheological Characterisation of Ceramic Inks for 3D Direct Ink Writing: A Review. *J. Eur. Ceram. Soc.* **2021**, *41*, 18–33. [CrossRef]

Disclaimer/Publisher's Note: The statements, opinions and data contained in all publications are solely those of the individual author(s) and contributor(s) and not of MDPI and/or the editor(s). MDPI and/or the editor(s) disclaim responsibility for any injury to people or property resulting from any ideas, methods, instructions or products referred to in the content.